Journal of Sound and Vibration (2001) **244**(1), 107–122
doi:10.1006/jsvi.2000.3460, available online at http://www.idealibrary.com on IDEAL®

ACTIVE CONTROL OF ENVIRONMENTAL NOISE, V: THE EFFECT OF ENVIRONMENT CHANGE ON THE STABILITY OF ELECTRONICALLY CONTROLLED ACOUSTIC SHADOW SYSTEMS

S. E. Wright and H. Atmoko

*School of Engineering, University of Huddersfield, Huddersfield HD*1 3*DH, England.*
E-mail: selwyn.wright@ntlworld.com

(*Received* 28 *May* 1999, *and in final form* 19 *October* 2000)

This paper considers the effect of environmental change on the stability of hardware implemented electronically controlled acoustic shadow (ECAS) systems. These systems generate quiet zones (acoustic shadows) from unwanted noise sources in unrestricted space. The acoustic transfer function of the system representing the acoustic environment is measured by using white noise impulse response techniques. The change in this function compared to the free field stationary propagating fluid value is determined. The effect of this change on the system stability is then expressed through the displacement of the stability region contours. This technique provides a method of measuring and correcting automatically for the displacement of the stability regions and thus maintaining the stability of the ECAS system through varying environmental conditions.

1. INTRODUCTION

In previous papers [1–4] in this series it has been shown, theoretically and through laboratory experiments, that active and adaptive electronically controlled acoustic shadow (ECAS) systems can produce wide, deep and long acoustic shadows. These systems, therefore, have the potential to reduce unwanted environmental noise. In reference [1] two-dimensional primary sources have been considered, radiating in free field (no reflections) in a propagating fluid at rest (no wind) by using computations based on wave theory. In reference [2] the effect of non-compact primary sources (high frequencies and/or large sources) has been considered. In reference [4] the effect of three-dimensional primary sources, out-of-phase primary sources, reflecting surfaces and steady wind have been considered, again by using wave theory computations. It has been shown in reference [3] how these wave systems can be implemented into practical hardware and how the stability of the adaptive process can be maximized. This paper considers the effect of acoustic environment change on the stability of these implemented systems, compared to free field, stationary propagating fluid conditions.

A sketch of a typical ECAS system, operating in free field, is shown in Figure 1. The primary sources (loudspeakers) provide the unwanted source to be cancelled. The secondary sources (loudspeakers) provide the cancellation and the detectors (microphones) monitor the system. The successive alignment of the primary sources, secondary sources

0022-460X/01/260107 + 16 $35.00/0

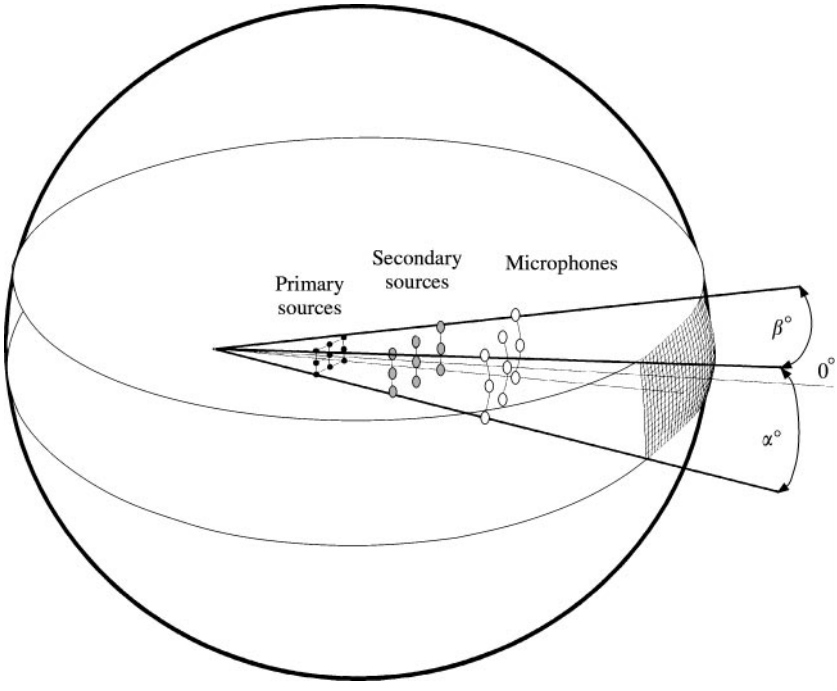

Figure 1. Electronically controlled acoustic shadow concept.

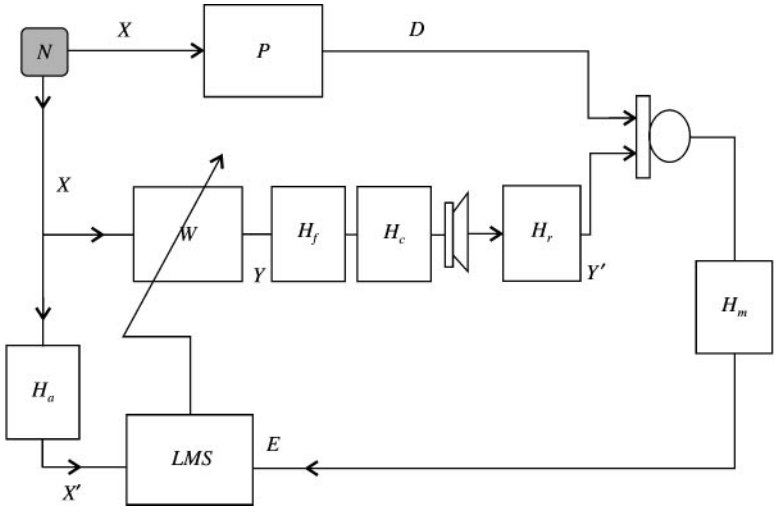

Figure 2. Practical control system.

and detectors lie within control angles α and β, that define the acoustic shadow angles. The electronic components of the system are illustrated diagrammatically in Figure 2. The function of the microphones is to receive signals from the acoustic waves being sent out from the source of unwanted noise and to instruct the secondary sources (loudspeakers) to send out acoustic waves in anti-phase so as to cancel the unwanted noise. It is physically obvious that the signals received by the microphones will depend on the acoustic

environment in which the system operates. Hence the stability of the overall ECAS system, including the microphones, cancelling loudspeakers, and the electronic controller will depend on the acoustic environment.

In section 2, a model of the overall system is presented in terms of the system's electromechanical and acoustic transfer functions. It is shown how the acoustic part of the transfer function changes depending on the acoustic environment in which the ECAS system operates. Accordingly, it is found how these changes can be determined by appropriate measurements, how these changes affect the stability of the adaptive system and how appropriate action can be taken. In section 3, the details of acoustic environment transfer functions are considered for two simple examples, namely an acoustically reflecting/absorbing ground surface and a reflecting back wall. These individual examples are not important; they serve only to show, in general, how the environment affects the acoustic system transfer function compared to that in free field conditions.

2. INFLUENCE OF ACOUSTIC ENVIRONMENT

2.1. A PRACTICAL CONTROL SYSTEM

Figure 2 shows the schematic diagram of a practical control system considered in detail in reference [3]. The functions H_f, H_c and H_m represent the transfer functions of the signal conditioning filters, secondary cancelling sources (speakers) and detection microphones, respectively. H_r is the transfer function representing the propagation distance between the secondary sources and microphones, which is equivalent to a phase retardation. P is the primary source propagation path. For a single discrete frequency, the weight adjustment filter W can be adequately implemented as a 2 tap FIR filter with the use of the delayed LMS algorithm.

For the system to cancel, the secondary source path X to Y' has to be equal to the primary source path X to D. W is adjusted until $D = Y'$ making $E \to 0$ at the error microphone, whose transfer function is common to both paths. The total transfer function around the control loop Y–E is then

$$H_{ttf} = \frac{Y'}{Y}\frac{E}{Y'} = \frac{E}{Y} = H_f H_c H_m H_r. \tag{1}$$

A further phase term is introduced through the delayed LMS algorithm, that can effectively offset the propagation delay term H_r. This introduces a fifth transfer function H_a that is equivalent to a phase advance, making the effective total transfer function around the loop

$$H_{ttf} = H_{em} H_r H_a \quad \text{where} \quad H_{em} = H_f H_c H_m. \tag{2}$$

H_{em} now represents the electromechanical transfer function of the system.

2.2. CONTROL SYSTEM STABILITY

Although the stability of a control system depends on both the amplitude and phase of its transfer functions, it is the phase that determines the stability region positions. Further background information regarding the stability of active noise control systems can be found in references [5–7]. Basically the adaptive loop illustrated in Figure 2, is convergent when the phase angle ϕ of equation (2) is within $\pm \pi/2$ of an integer number N of 2π radians,

which are referred to as stability regions (bands): i.e.,

$$\phi = \angle H = \pi + 2\pi N \pm \pi/2, \quad N = 0, \pm 1, 2, \ldots . \tag{3}$$

The π ensures cancellation of the primary field. From equation (2), the total phase transfer function, in terms of the number N, becomes

$$N_{ttf} = N_{tf} + N_a, \quad \text{where} \quad N_{tf} = N_{em} - N_r. \tag{4}$$

N_{tf} is the phase transfer function of the system; it includes the electromechanical and propagation delay functions. It is shown for a real system in reference [3] that

$$N_r = r_{sm}/\lambda_{ac} = r_{sm} f_{ac}/c_0, \qquad N_a = n_a/n_{ac} = n_a f_{ac}/f_n. \tag{5}$$

N_r is the number of acoustic wavelengths λ_{ac} in the propagation distance r_{sm} between the secondary speaker and the detection microphone. N_a is the ratio of the sample advance number n_a used in the delayed LMS, and the ratio of the sampling and acoustic frequency f_n/f_{ac}, c_0 is the speed of sound taken to be 340 m/s. Equation (4) then becomes

$$N_{ttf} = N_{tf} + n_a f_{ac}/f_n = \left(\frac{n_a}{f_n} - \frac{r_{sm}}{c_0} \right) f_{ac} + N_{em}. \tag{6}$$

The electromechanical phase transfer function N_{em} can be obtained from the measured total phase transfer function of the system N_{ttf}. This occurs when the sample advance number n_a in the LMS algorithm and the propagation distance r_{sm} is zero (microphone in close contact with the secondary speaker) i.e.,

$$N_{em} = N_{ttf} \quad \text{when} \quad N_r = N_a = 0, \quad \text{i.e. } r_{sm} = n_a = 0. \tag{7}$$

N_{ttf} and N_{em} are defined initially for freefield (anechoic) conditions. However, these functions can be extended to cover environmental conditions such as reflections and wind. Here one defines an environmentally modified electromechanical transfer function N_{emr} such that

$$N_{emr} = N_{ttf} \quad \text{when} \quad N_r = N_a, \quad \text{i.e. from equation (5) } n_a = r_{sm} f_n/c_0 \tag{8}$$

$$\text{or } N_{ttf} = N_{tf} = N_{emr} - N_r \quad \text{from equation (4) when } N_a = 0, \text{ i.e. } n_a = 0. \tag{9}$$

In either case, propagation space is involved ($r_{sm} \neq 0$) which can be modified by environmental changes. The pure delay part of N_r is removed from N_{ttf}, either by offsetting it with the sample advance number as in equation (8), or by effectively adding it as in equation (9). The remaining propagation effects such as reflections, wind, etc., are now contained in N_{emr}. This modified electromechanical transfer function concept is very useful as it includes (has in-built) the effect of any environmental deviations from the freefield condition.

2.3. THE IMPULSE RESPONSE

The factor representing the effects of the acoustic environment has been identified theoretically. The question is how to measure it in practice. Consider first the impulse response, which can be used to measure the transfer functions of the system. Figure 3 shows

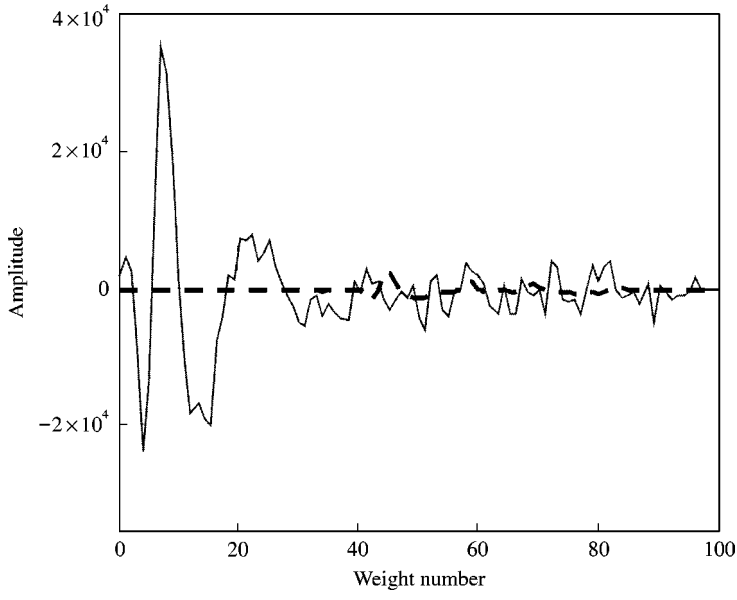

Figure 3. Impulse responses $I_{em}(r_{sm} \approx 0)$ (—) and $I_{tf}(r_{sm} = 3{\cdot}23\text{ m})$ (– – –).

the typical impulse responses for a single channel system. They are generated by a white noise system identification procedure, using an FIR filter with 86 taps (weights), 1000 samples and a sampling frequency of 4000 samples per second, resulting in a 0·25 s broadband tone burst. Provided a sufficiently large number of weights (filter taps) are used, the number of weights becomes equivalent to the number of samples in the time domain.

The first impulse response, I_{em}, is measured with the microphone in close contact with the secondary loud speaker ($r_{sm} \approx 0$). This is used to obtain the electromechanical transfer function of the system alone, according to equation (7). The second impulse, I_{tf}, is measured at a speaker–microphone distance $r_{sm} = 3{\cdot}23$ m. This measures the system response, including the transfer function of the propagation space between the speaker and the microphone, according to equation (9). The second response is weaker because of the further propagation distance.

2.4. THE PROPAGATION DISTANCE

The secondary speaker–microphone distances r_{sm} can be calculated or measured directly from the system geometry. Or they can be calculated from the measured impulse response files, by using MATHCAD or some other equivalent software. This is particularly useful, if a large number of channels is used. The number of propagation paths increases as the square of the channel number (8 channels ≡ 64 paths, which is a large number of paths to measure accurately).

In the software approach, the maximum value of the impulse response is sought and then the corresponding sample number (weight number i) of a predetermined fraction of the maximum value is found (17% in this case). This corresponds to 3 and 41 sample numbers from equations (12) and (13) below, for I_{em} and I_{tf} respectively. The respective propagation distances are then calculated from equations (14) and (15) as 0·0 and 3·23 m. The minus 3 sample numbers are included to anticipate the start of the impulses before the 17% value.

The white noise data files are as follows:

$$I_{em} = \text{READPRN (trfn\_0)}, \qquad I_{tf} = \text{READPRN (s2m6\_86t)} \tag{10}$$

$$\text{detect}(I) = \left| \begin{array}{l} i \leftarrow 0 \\ \text{while } |I_i| < \dfrac{|\max(I)|}{6} \\ \quad i \leftarrow i + 1 \\ i \end{array} \right. \tag{11}$$

$$\max(I_{em}) = 3{\cdot}577 \times 10^4, \qquad \text{detect}(I_{em}) = 3, \tag{12}$$

$$\max(I_{tf}) = 2{\cdot}455 \times 10^3, \qquad \text{detect}(I_{tf}) = 41, \tag{13}$$

$$r_{sm1} = \frac{(\text{detect}(I_{em}) - 3) \times 340}{4000}, \qquad r_{sm1} = 0, \tag{14}$$

$$r_{sm2} = \frac{(\text{detect}(I_{tf}) - 3) \times 340}{4000}, \qquad r_{sm2} = 3{\cdot}23. \tag{15}$$

2.5. THE GAIN RESPONSE

Next, one can consider the gain responses calculated from the impulse responses in equations (16) and (17). In the MATHCAD software formulation, the sampling frequency $f_n = 4$ kHz, the discrete integer labeled j is a frequency integer, giving a frequency range of 1–1000 Hz, and x_j is a Nyquist ratio variable. G_{em} and G_{tf} are the gain (amplitude) responses:

$$f_n = 4000, \qquad j = 1\text{–}1000, \qquad x_j = \frac{j}{4000}, \qquad f_j = x_j \cdot f_n, \tag{16}$$

$$G_{em_j} = |\text{gain}(I_{em}, x_j)|, \qquad G_{tf_j} = |\text{gain}(I_{tf}, x_j)|. \tag{17}$$

Figure 4 shows the amplitude responses of the electromechanical G_{em} and the system G_{tf} transfer functions. It can be seen that the gain of the system falls off rapidly below 200 Hz (approximately 20 dB down at 100 Hz) limited by the electromechanical transfer function of the secondary loudspeakers. The upper cut-off frequency (3 dB down point) is about 800 Hz, dominated by the antializing/quantization filter in the computer.

2.6. THE PHASE RESPONSE

Figure 5 shows the phase responses for the electromechanical N_{em} and system N_{tf} transfer functions, calculated by equations (18) and (19), for propagation distances $r_{sm} = 0$ and 3·23 m respectively. Here the phase angle argument is calculated first (wrapped phase) from the impulse response. Then the phase is unwrapped (phasecor) and divided into N 2π

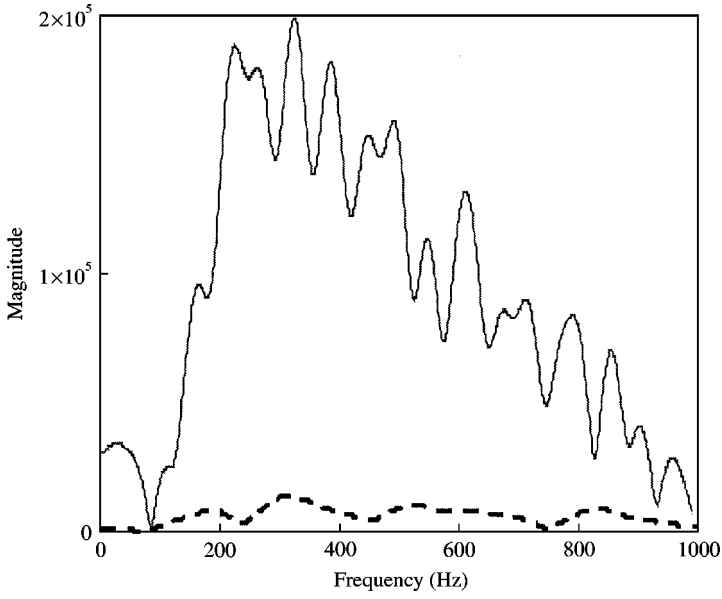

Figure 4. Magnitude response of G_{em} (—) and G_{tf} (– –).

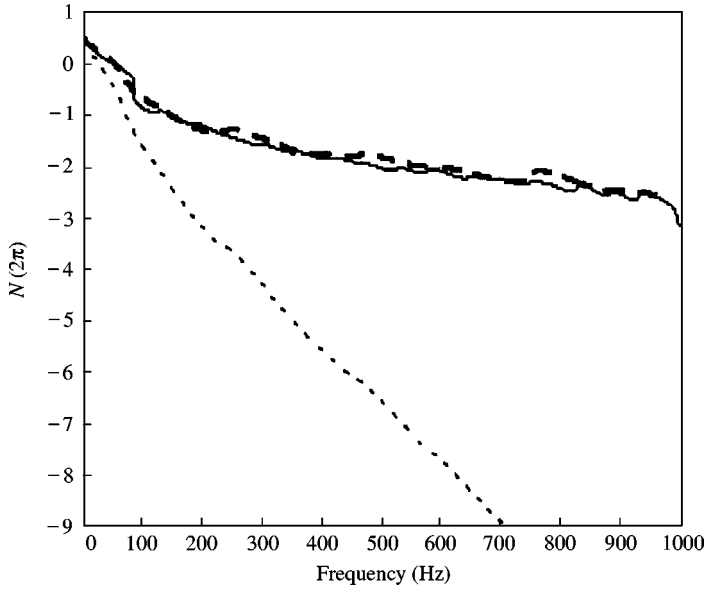

Figure 5. Phase transfer functions. System transfer function N_{tf} (- -), actual electromechanical N_{em} (——) and environmentally modified electromechanical by reflection N_{emr}(– –).

stability regions.

$$\Phi_{em_j} = \arg(\text{gain}(I_{em}, x_j)), \qquad N_{em} = \frac{\text{phasecor}(\Phi_{em})}{2\pi}, \tag{18}$$

$$\Phi_{tf_j} = \arg(\text{gain}(I_{tf}, x_j)), \qquad N_{tf} = \frac{\text{phasecor}(\Phi_{tf})}{2\pi}. \tag{19}$$

In the figure, the curves start from $N = -0{\cdot}5(-\pi)$ corresponding to an antiphase cancelling system. The electromechanical system phase response N_{em} can be seen to decay from a $0{\cdot}5N$ to $3{\cdot}5N$, i.e. $3N$ or 6π over a frequency range of 1 kHz. A good approximation for this function is

$$\Phi_{em} = \angle(1 + j\omega\tau)^{-p}. \tag{20}$$

In the above equation $\tau \approx 1$ ms, is the effective time constant of the system and $p \approx 13$ is the total electrical multipole order including AD and DA filters. The system phase transfer function N_{tf}, given by equations (5) and (9), is seen to drop rapidly, dominated by the propagation phase lag term N_r. The environmentally modified electromechanical transfer function N_{emr}, is also shown in Figure 5. It is computed from equation (21) below from the system transfer function N_{tf} plus the propagation term N_r, as given by equation (9):

$$N_{emr} = \frac{r_{sm2}}{c_0} f + N_{tf}. \tag{21}$$

For non-reflecting (anechoic) surroundings, the environmentally modified function N_{emr} compares favourably with the function based solely on the electromechanical transfer function N_{em}. This provides a method of evaluating (and in this case confirming) the anechoic properties of the chamber.

2.7. STABILITY REGION CONTOURS

The contours of the center of the stability regions can be found by using integer values in the total phase transfer function N_{ttf}, i.e., $N_{ttf} \to N$ in equation (6). Rearrangement of this equation gives

$$n_a = (N - N_{tf}) f_n / f_{ac} = \left(\frac{N - N_{em}}{f_{ac}} + \frac{r_{sm}}{c_0} \right) f_n. \tag{22}$$

Again n_a is the sample advance number in the delayed LMS algorithm and f_{ac}, is the acoustic frequency. Any stability region number N can be 'tuned in', for a given operating set-up, by selecting the appropriate n_a number given by the above equation.

The stability region map of the control system as computed for anechoic conditions is shown in Figure 6. N_{em} is the electromechanical transfer function, measured as a function of frequency in the previous section. The figure shows the stability region contours, plotted for N values from 4 to -4, for a range of n_a numbers from 0 to 80. For a given frequency f_{ac} and stability number N, the corresponding n_a number, to give system stability, can be read from the figure. From equation (8) the electromechanical transfer function N_{em} as a function of frequency, can be read across the figure. For $r_{sm} = 3{\cdot}23$ m, $f_n = 4$ kHz and $c_0 = 340$ m/s, the corresponding sample number is

$$n_a = n_r = r_{sm} f_n / c_0 = 38. \tag{23}$$

If the propagation space is not anechoic, then the environmentally modified electromechanical transfer function, N_{emr}, equation (9), is used in place of N_{em} in equation (22). Any deviation from an otherwise anechoic propagation space will manifest itself in changes in N_{emr} and then in changes in the positions of the stability region contours. These

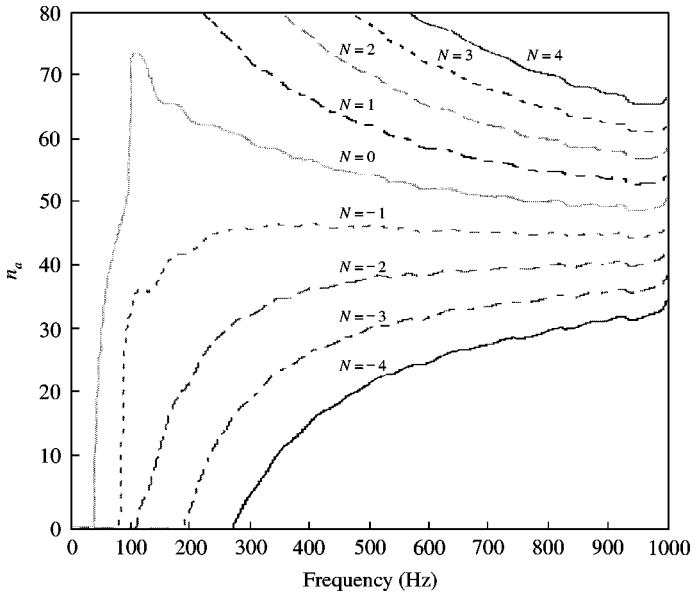

Figure 6. Stability region contours using the electromechanical transfer function N_{em} shown in Figure 5 ($r_{sm} = 3{\cdot}23$ m).

changes, if not corrected for, will affect the performance of the adaptive process. Shifts in these stability region contours provide an analytical, as well as a visual measure of the relative stability region distortion produced by the environmentally modified propagation space, compared to freefield (anechoic) condition.

3. EXAMPLES OF ENVIRONMENTAL EFFECTS

The previous section has indicated how the effect of the propagation space (acoustic environment in which the cancelling system is operating) affects the total system transfer function, how it can be measured, and how it can affect the stability of the adaptive process (distortion of stability region contours). Two examples are now considered.

3.1. EFFECT OF GROUND REFLECTION

As a simple example, the effect of floor (ground) reflection is computed, by measuring N_{emr} with and without acoustic absorbing treatment on the floor. The two following data files correspond to a source–microphone distance $r_{sm} = 3$ m, at a height $h = 1{\cdot}75$ m above the floor, with and without acoustic treatment:

$$W_{r1} := \text{READPRN (t2b1d2e3)}, \qquad W_{r2} := \text{READPRN (u2b1d2e3)}. \tag{24}$$

Figure 7 shows the impulse responses for the two data files. The reflected pulse W_2, from the untreated floor, can be seen clearly arriving at about 19 FIR tap (sample) numbers later than the original direct pulse path W_1. This translates into a propagation path difference of

$$\Delta r = i\, c_0/f_n = 19 \times 340/4000 = 1{\cdot}6 \text{ m}, \tag{25}$$

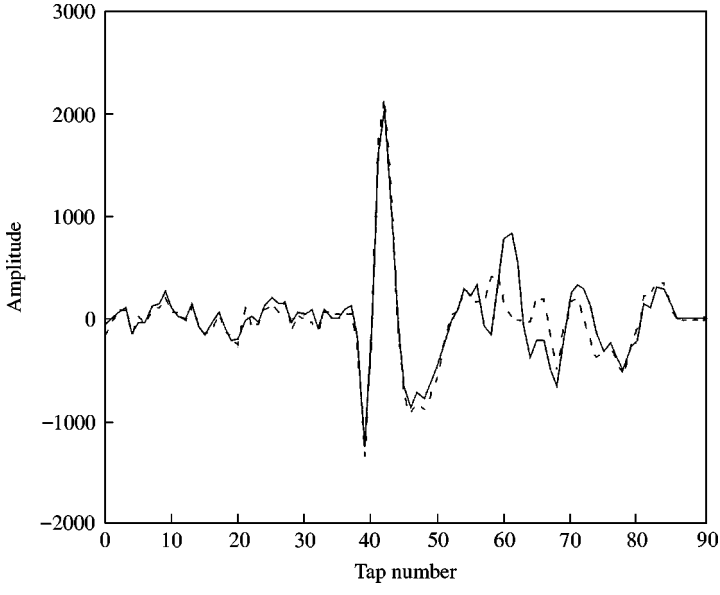

Figure 7. Impulse response for non-reflecting W_1 (– –) and reflecting floor W_2 ($r_{sm} = 3$ m) (—).

which is in agreement with the system/room geometry path difference of

$$\Delta r = [(2h)^2 + r_{sm}^2]^{1/2} - r_{sm} = [3{\cdot}5^2 + 3^2]^{1/2} - 3 = 1{\cdot}6 \text{ m}. \tag{26}$$

Figure 8 shows the resulting amplitude responses. Here interference minima for the reflecting floor are clearly seen (solid line) at about 315, 525 and 735 Hz, formed by multiples of π phase differences between the direct and reflected propagation paths. This corresponds to the destructive interference for $3\lambda/2$, $5\lambda/2$ and $7\lambda/2$, where λ is the acoustic wavelength ($\lambda/2$ is below the system response). Constructive interference occurs for multiples of 2π phase differences, giving maxima, not so clearly seen, at 210, 420, 630 and 840 Hz, giving an acoustic wavelength of

$$\lambda = c_0/f_{ac} = 340/210 = 1{\cdot}6 \text{ m} \tag{27}$$

i.e., the same length as the path difference calculated from the delayed impulse response, equation (25), and the system geometry, equation (26).

Figure 9 shows the environmentally modified electromechanical phase transfer functions corresponding to the treated floor N_{emr1} and untreated floor N_{emr2}, obtained by using equations (5) and (9) or (21). The effect of the deepest interference minima in Figure 8, occurring at about 315 and 735 Hz, are carried over and clearly visible for the reflecting floor case in Figure 9. Local phase deviations $\approx \pi/2$ radians can be seen (N integer is equal to 2π radians).

The corresponding stability region contours are plotted in Figures 10 and 11 for the non-reflecting and reflecting floor case. Again local deviations, but now reversed, are carried over into the stability region contours. The maximum deviations, corresponding to reflection, compared with the anechoic case, are about 5 n_a numbers equivalent to about $N/2 = \pi$ radians. The deviations reduce in relative size with reducing n_a or N number. Note that the vertical separation between the N contours is constant for a given frequency.

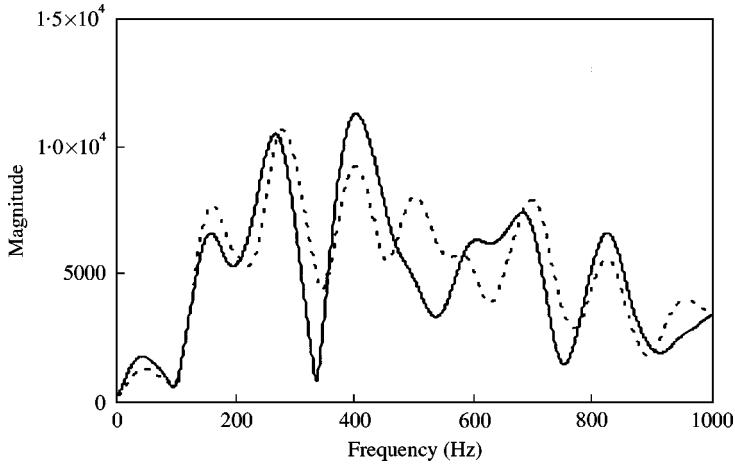

Figure 8. Magnitude response for non-reflecting G_1 (– –) and reflecting floor G_2 (—).

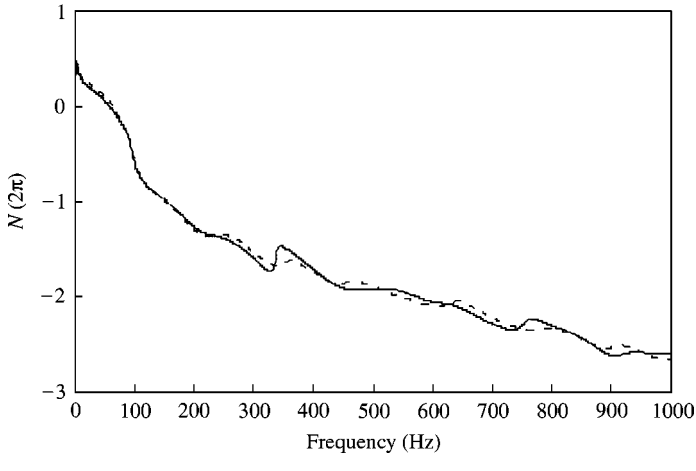

Figure 9. Environmentally modified electromechanical phase transfer functions for non-reflecting floor N_{emr1} (– – –) and reflecting floor N_{emr2} (—)

3.2. EFFECT OF BACK WALL REFLECTION

Forward wall reflection can be treated similarly to forward ground reflection. The effect of vertical rear wall reflection usually results in multiple reflections, as sound bounces back and forth between the cancelling system and the wall or surface. This provides a more complex acoustic environment to analyze.

The following three data files are taken with a reflecting back wall 0·35 m behind the speaker, for speaker–microphone distances of nominally 1, 2 and 3 m. The transducers are at a height of about 1·75 m above an acoustically treated floor.

The maximum pulse amplitudes and distances (in sample numbers and metres) between the speaker and microphone for the three files are as follows:

$$W_{r1} = \text{READPRN (t1b1d2e1)}, \quad \max(W_{r1}) = 2{\cdot}05 \times 10^3, \quad \text{detect}(W_{r1}) = 15, \quad r_{sm1} = 0{\cdot}935; \tag{28}$$

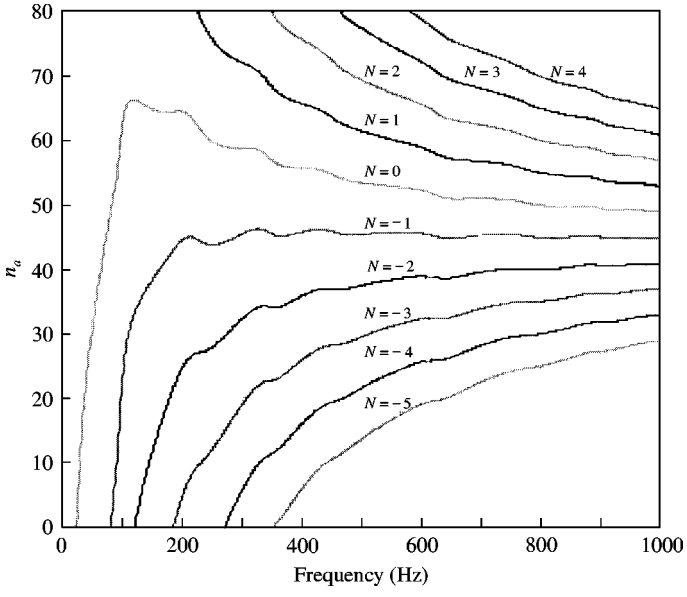

Figure 10. Stability region contours for non-reflecting floor N_{emr1} ($r_{sm} = 3$ m).

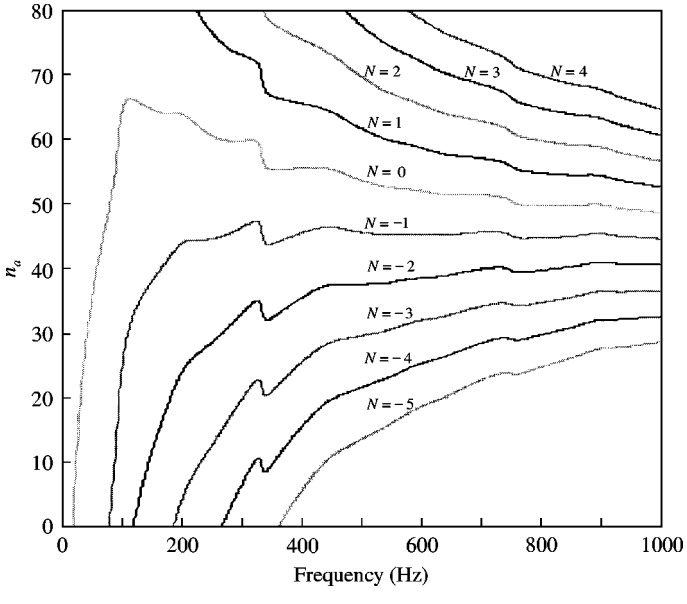

Figure 11. Stability region contours for reflecting floor N_{emr2} ($r_{sm} = 3$ m).

$$W_{r2} = \text{READPRN (t1b1d2e2)}, \quad \max(W_{r2}) = 1{\cdot}86 \times 10^3, \quad \text{detect}(W_{r2}) = 27, \quad r_{sm2} = 1{\cdot}955; \tag{29}$$

$$W_{r3} = \text{READPRN (t1b1d2e3)}, \quad \max(W_{r3}) = 1{\cdot}565 \times 10^3, \quad \text{detect}(W_{r3}) = 38, \quad r_{sm3} = 2{\cdot}89. \tag{30}$$

Figure 12 shows the impulse responses for the three speaker–microphone distances. Note the series of multiple reflections for each distance. The reflections are separated by about

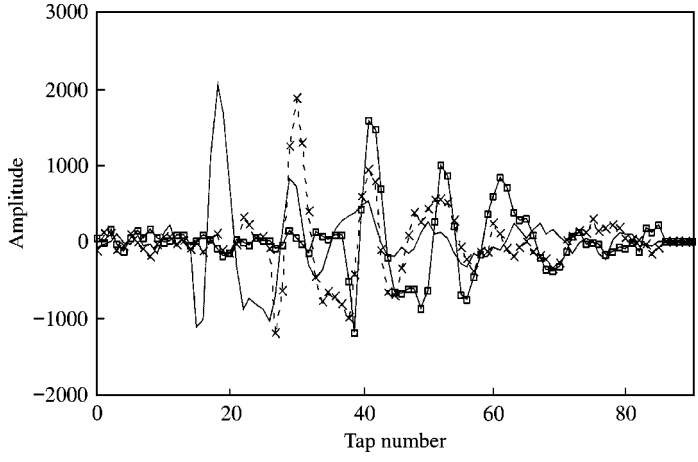

Figure 12. Impulse response W_1 ($r_{sm} = 1$ m) (—), W_2 ($r_{sm} = 2$ m) (– × –), and W_3 ($r_{sm} = 3$ m) (–□–).

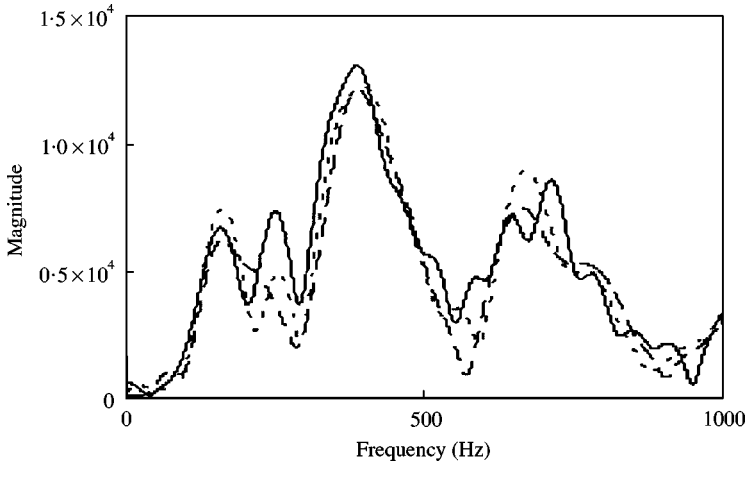

Figure 13. Magnitude response of G_1 ($r_{sm} = 1$ m) (—), G_2 ($r_{sm} = 2$ m) (- -), and G_3 ($r_{sm} = 3$ m) (– –).

eight samples (nearest whole sample) corresponding to a path difference of about $\Delta r = i\, c_0/f_n = 9{\cdot}340/4000 = 0{\cdot}8$ m. This corresponds to the measured speaker–wall distance of about 0·4 m.

Figure 13 shows the amplitude responses for the three different distances. Destructive interference occurs for all three functions at about 185, 555, 925 Hz which corresponds to $\lambda/2$, $3\lambda/2$ and $5\lambda/2$. Also, constructive reinforcement occurs at about 370, 740 Hz, which corresponds to acoustic wavelengths of λ and 2λ. This gives an approximate propagation path difference of $\Delta r = \lambda = c_0/f_{ac} = 0{\cdot}9$ m, which is a little more than twice the speaker–wall distance of about 0·4 m.

Figure 14 gives the unwrapped phase transfer function responses N_{tf}, for the four distances, where the spectrum gradients increase with speaker–microphone distance r_{sm}, according to equations (5) and (9). The apparently random phase calculations below the lower cut-off frequency of the electromechanical system, (approximately 100 Hz), have little significance. The dominant minima in Figure 13, at about 300, 555 and 925 Hz, give corresponding phase deviations which can just about be detected in Figure 14.

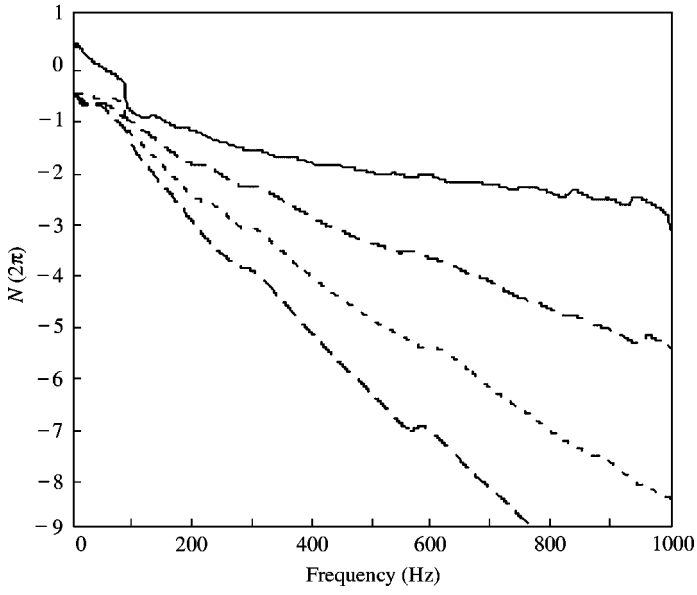

Figure 14. Phase response of N_1 ($r_{sm} = 1$ m) (——), N_2 ($r_{sm} = 2$ m) (– – – –), N_3 ($r_{sm} = 3$ m) (– · – · –) and N_4 ($r_{sm} = 0$ (– – –).

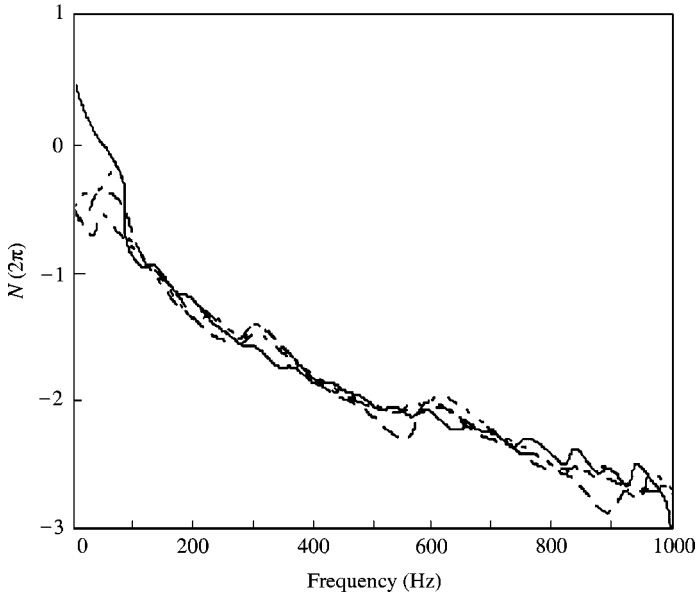

Figure 15. Modified electromechanical phase transfer functions N_{emr1} ($r_{sm} = 1$ m) (– · – · –), N_{emr2} ($r_{sm} = 2$ m) (– –), N_{emr3} ($r_{sm} = 3$ m) (——) and N_{emr4} ($r_{sm} = 0$) (—).

Figure 15 shows the environmentally modified phase transfer functions given by equation (31) below for those functions given in Figure 14. These are derived from equation (21) where the r_{sm} distances are given in equations (28)–(30)

$$N_{emr1} := \frac{r_{sm1}}{340} f + N_1, \qquad N_{emr2} := \frac{r_{sm2}}{340} f + N_2, \qquad N_{emr3} := \frac{r_{sm3}}{340} f + N_3. \tag{31}$$

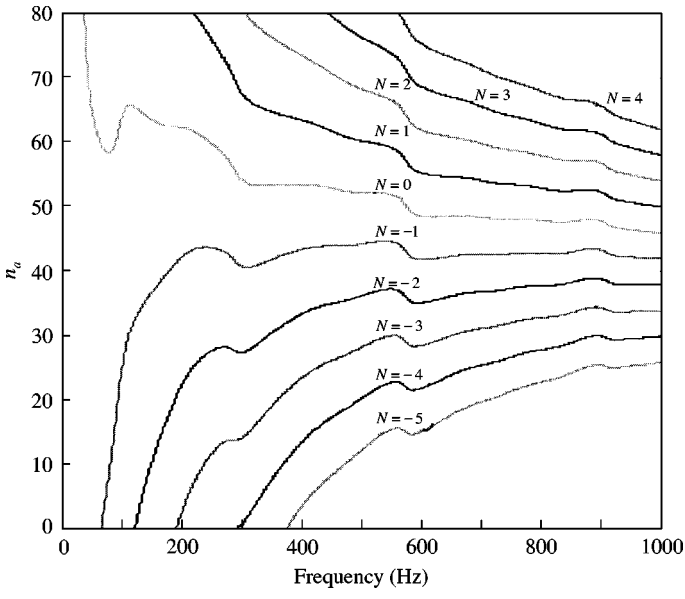

Figure 16. Stability region contours for back wall reflections N_{emr3} ($r_{sm} = 3$ m).

Again phase deviations of about $\pi/2$ can be seen. Finally, Figure 16 shows the corresponding phase deviation being carried through into the stability region contour, for example, N_{emr3}. By comparing this with Figure 10 for anechoic conditions, it can be seen that there is considerable stability region distortion.

4. DISCUSSION

The effect of environmental changes on the stability of the adaptive process could be abrupt or smoothly changing: e.g., gusting winds, temperature changes, intermittent rain/snow showers, increasing fog, changing ground cover or moving surfaces. Whatever the environmental change the effect is felt through a change in the acoustic transfer function. In fact the actual environmental change is not important and does not need to be known, just its magnitude and phase effect on the acoustic transfer function. Initially the stability conditions are set so that the system is operating at the centre of its stability bands in a free field stationary propagating fluid situation.

Any environmental change then affects the acoustic transfer function, displacing the stability region contours compared to their freefield stationary propagating fluid positions. These stability region changes can be measured automatically, and corrections made to return the contours to their original position, so that the system is again operating in the centre of its stability band. This can be accomplished without any further environmental information being known or measured, such as temperature, wind velocity, ground impedance, or ground obstructions, etc.

These corrective actions have to be made in real time for the system to remain stable. The sampling frequency used is usually 4 kHz (updating time 0·25 ms) for a 100–1000 Hz band width, satisfying well the Nyquist sampling criteria. The stability region widths, given approximately by f_n/f_{ac}, are at least five samples wide for an acoustic frequency $f_{ac} = 400$ Hz. This is considered adequate resolution to maintain the stability region close to the centre of its stability band.

The execution time of the TI processor is a fraction of a nano-second. The adaptive algorithm of a few hundred executions requires, therefore, a total processing time of less than 0·1 μs, well under the sampling time of 0·25 ms. The adaptive theory and speed for a single channel system is considered in reference [8] and a publication on multi-channel systems is under preparation. The adaptive time constant of these systems is of the order of 10 samples (2·5 ms). This depends on the adaptive step size, reference signal strength, cancelling frequency, microphone propagation distance, channel number, source array size and other geometric conditions.

Usually environmental changes are considerably slower than this. In large enclosed spaces such as factories there are few environmental changes; usually moving surfaces and people constitute the main problem. In the open air, environmental changes are usually slow except for high winds where the system is usually not required because the wind noise then dominates. Patents for the implementation of these corrective actions have been applied for and therefore cannot be discussed further.

5. CONCLUSION

The transfer functions and resulting stability regions for electronically controlled acoustic shadow systems operating in three-dimensional space have been investigated. To operate these systems efficiently (deep shadows, high adaptive speeds and low spectrum distortion) it is essential to be able to predict and operate close to the centre of these stability regions. Changes in these regions through propagation effects should be anticipated and appropriately corrected for, otherwise inferior system performance or even system instability could result. It is shown how these functions and the effect of environmental change on these functions can be measured and how corrections can be made to maintain stability.

REFERENCES

1. S. E. WRIGHT and B. VUKSANOVIC 1996 *Journal of Sound and Vibration* **190**, 565–585. Active control of environmental noise, I.
2. S. E. WRIGHT and B. VUKSANOVIC 1997 *Journal of Sound and Vibration* **202**, 313–359. Active control of environmental noise, II: non-compact acoustic sources.
3. S. E. WRIGHT and B. VUKSANOVIC 1999 *Journal of Sound and Vibration* **220**, 469–496. Active control of environmental noise, III: implementation of theory into practice.
4. S. E. WRIGHT and B. VUKSANOVIC 1999 *Journal of Sound and Vibration* **222**, 635–668. Active control of environmental noise, IV: practical extensions to ECAS theory.
5. B. WIDROW and S.D STEARNS 1995 *Adaptive Signal Processing*. Englewood Cliffs NJ: Prentice-Hall.
6. P. F. FEINUTCH, N. J. BERSHAD and A. K. LO 1993 *IEEE Transactions on Signal Processing* **41**, 1518–1531. A frequency domain model for "filtered" LMS algorithms—stability analysis, design and elimination of the training mode.
7. S. D. SNYDER and C. H. HANSEN 1994 *IEEE Transactions on Signal Processing* **42**, 950–953. The effect of transfer function estimation errors on filtered X LMS algorithm.
8. S. E. WRIGHT and H. ATMOKO 2000 *Journal of Sound and Vibration* Accepted for publication. Active control of environmental noise, VI: adaptive and acoustic performance of a fundamental free-field cancelling system.